

Anomalous metallic phase in tunable destructive superconductors

S. Vaitiekėnas , P. Krogstrup, and C. M. Marcus *Center for Quantum Devices and Microsoft Quantum Lab–Copenhagen, Niels Bohr Institute, University of Copenhagen, 2100 Copenhagen, Denmark*

(Received 2 October 2019; revised manuscript received 3 January 2020; accepted 6 February 2020; published 26 February 2020)

Multiply connected superconductors smaller than the coherence length show destructive superconductivity, characterized by reentrant quantum phase transitions driven by magnetic flux. We investigate the dependence of destructive superconductivity on flux, transverse magnetic field, temperature, and current in InAs nanowires with a surrounding epitaxial Al shell, finding excellent agreement with mean-field theory across multiple reentrant transitions. Near the crossover between destructive and nondestructive regimes, an anomalous metal phase is observed with temperature-independent resistance, controlled over two orders of magnitude by a millitesla-scale transverse magnetic field.

DOI: [10.1103/PhysRevB.101.060507](https://doi.org/10.1103/PhysRevB.101.060507)

Quantum phase transitions [1,2] in conventional superconductors serve as prototypes for related effects in more complex, strongly correlated systems [3], including heavy-fermion materials [4] and high-temperature superconductors [5]. While low-temperature superconductors are well understood in bulk, new phenomena can arise in mesoscopic samples and reduced dimensionality [6,7]. For instance, in two-dimensional films, electrons theoretically condense into either a superconductor or insulator in the low-temperature limit [8]. Yet, in many instances, an anomalous metallic state with temperature-independent resistance is found at low temperatures [9]. In one-dimensional wires, incoherent phase slips can destroy superconductivity [10] or give rise to an anomalous metallic state [11], while coherent quantum phase slips can lead to superposition of quantum states enclosing different numbers of flux quanta [12], potentially useful as a qubit [13].

Multiply connected superconductors provide an even richer platform for investigating phase transitions. Fluxoid quantization in units of $\Phi_0 = h/2e$ [14,15], reveals not only electron pairing but a complex macroscopic order parameter, $\Delta e^{i\varphi}$ [6,16]. The same physical mechanism underlies the Little-Parks effect, a periodic modulation of the transition temperature, T_C , of a superconducting cylinder with magnetic flux period Φ_0 [17]. For hollow superconducting cylinders with diameter, d , smaller than the coherence length, the modulation amplitude can exceed zero-field transition temperature, T_{C0} , leading to a reentrant destruction of superconductivity near odd half-integer multiples of Φ_0 [18–20].

Early experimental investigation of the destructive Little-Parks effect reported reentrant superconductivity interrupted by an anomalous-resistance phase around applied flux $\Phi_0/2$ [21]. Subsequent experiments showed a low-temperature phase with normal-state resistance, R_N , around $\Phi_0/2$, but did not display fully recovered superconductivity at higher flux [22]. Several theoretical models were proposed to interpret these different scenarios [23–25], but no consensus emerged.

Here, we report a study of the Little-Parks effect across the transition from destructive to nondestructive regimes, in InAs nanowires with a thin epitaxial cylindrical Al shell. Remarkable agreement with Ginzburg-Landau mean-field theory is observed across multiple reentrant lobes as a function of flux, temperature, and current bias, using independently measured material and device parameters. We then investigate a field-tunable crossover from nondestructive to destructive regime. At the boundary, an anomalous metal phase is identified, characterized by a temperature-independent resistance that can be tuned over two orders of magnitude using small changes in perpendicular magnetic field, B_\perp . We interpret these results in terms of tunneling between adjacent fluxoid states with different phase winding numbers giving rise to an anomalous metallic phase. As noted previously [24], the appearance of a field-tunable temperature-independent resistance does not emerge naturally from simple models. The basic mechanism leading to a field-tunable saturating resistance remains mysterious.

The devices we investigated were made using InAs nanowire grown by the vapor-liquid-solid method using molecular beam epitaxy (MBE). Following wire growth, an

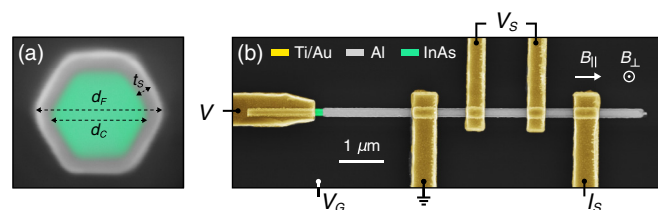


FIG. 1. (a) Colorized material-sensitive scanning electron micrograph of InAs-Al hybrid nanowire cross section. The full wire diameter d_f , core diameter d_c , and shell thickness t_s are indicated by dashed arrows. (b) Representative color-enhanced micrograph of a device (wire B) consisting of an InAs core (green) with Al shell (gray), contacted with Ti/Au leads (yellow). The device can be operated in voltage (V) and current (I_s) bias measurement setups.

epitaxial Al layer was grown within the MBE chamber while rotating the sample stage, resulting in a full cylindrical Al shell coating the wire [26], as shown in Fig. 1(a). Subsequent fabrication used standard electron-beam lithography, deposition, etching, and liftoff, as described elsewhere [27]. Devices were operated in two configurations [Fig. 1(b)]: In the first configuration, four Au contacts were made to the Al shell allowing four-wire resistance measurements; in the second, an additional tunneling contact to the InAs core at the end of the wire was used as a tunnel probe, giving local density of states, as discussed in Ref. [27]. We investigated wires from three growth batches, denoted A, B, and C, with different core diameters, d_C , and shell thicknesses, t_S (see Supplemental Material [28]). Transport measurements were carried out in a dilution refrigerator with a three-axis vector magnet and base temperature of 20 mK.

Carrier density in the InAs core is predominantly at the Al interface due to band bending [30,31]. Moreover, the density of carriers in Al is orders of magnitude higher than in InAs. We may therefore consider current to be carried by a hollow cylinder which is threaded by flux in an axial applied magnetic field. Induced circumferential supercurrents from the applied flux lead to Cooper pair breaking, characterized by the parameter α , which controls the transition temperature $T_C(\alpha)$, as described by Abrikosov-Gorkov expression,

$$\ln\left(\frac{T_C(\alpha)}{T_{C0}}\right) = \Psi\left(\frac{1}{2}\right) - \Psi\left(\frac{1}{2} + \frac{\alpha}{2\pi k_B T_C(\alpha)}\right), \quad (1)$$

where Ψ is the digamma function [32]. Following Refs. [20,22,23], the pair-breaking parameter for a hollow cylinder with wall thickness t_S in a parallel magnetic field B_{\parallel} is given by

$$\alpha_{\parallel} = \frac{4\xi_S^2 T_{C0}}{A_F} \left[\left(n - \frac{\Phi}{\Phi_0}\right)^2 + \frac{t_S^2}{d_F^2} \left(\frac{\Phi^2}{\Phi_0^2} + \frac{n^2}{3}\right) \right], \quad (2)$$

where ξ_S is the zero-field superconducting coherence length, A_F is the area of the cylinder cross section, the integer n is the fluxoid quantum number, Φ is the applied flux, and d_F is the diameter of the cylinder [Fig. 1(a)]. Taking the dirty-limit expression for $\xi_S = \sqrt{\pi\hbar v_F l_e / 24k_B T_{C0}}$ with the Fermi velocity v_F and mean free path l_e , we note that all parameters can either be measured directly from the micrograph of the device or from independent transport measurements (see Supplemental Material [28]).

Differential shell resistances, $R_S = dV_S/dI_S$, for wires A and B are shown in Fig. 2 as a function of B_{\parallel} and temperature, T . Wires A and B have similar core diameters, $d_C \sim 135$ nm, but different shell thicknesses. For wire A, with $t_S = 7$ nm, T_C is finite throughout the measured range, and varies periodically with applied axial flux with amplitude ~ 0.4 K with no clear envelope reduction up to $B_{\parallel} = 0.4$ T. Normal-state resistance of the wire yields a coherence length $\xi_S = 70$ nm, smaller than d_C (see Supplemental Material [28]). In contrast, wire B, with $t_S = 25$ nm, has $\xi_S = 180$ nm $> d_C$, and shows destructive regimes around $\pm\Phi_0/2$ and $\pm 3\Phi_0/2$. Resistances in these destructive regimes remain equal to the normal-state resistance, $R_S = R_N$, to the lowest measured temperatures.

The absence (presence) of the destructive regime in wire A (B) is consistent with the criterion of the superconduct-

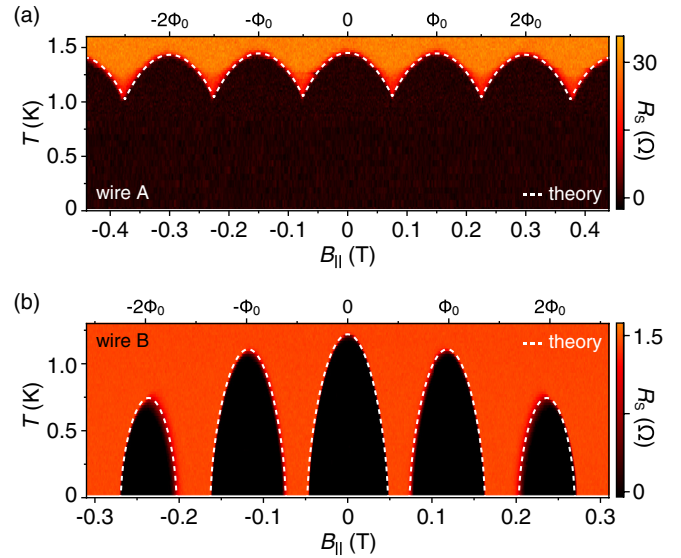


FIG. 2. (a) Shell resistance, R_S , measured for wire A with shell thickness $t_S = 7$ nm as a function of axial magnetic field, B_{\parallel} , and temperature, T . The superconducting transition temperature of the shell is periodically modulated by B_{\parallel} . The sample is superconducting for temperatures below 1 K throughout the whole measured B_{\parallel} range. The dashed theory curve is Eq. (1) evaluated with α_{\parallel} from Eq. (2) and the corresponding fit parameters measured for the wire A. (b) Same as (a), but measured for wire B with shell thickness around $t_S = 25$ nm, showing the destructive regimes around $\pm\Phi_0/2$ and $\pm 3\Phi_0/2$ of the applied flux quantum.

ing coherence length being smaller (larger) than the wire diameter [18]. To be more quantitative, we plot in Fig. 2 theoretical curves marking the superconductor-metal transition based on Eqs. (1) and (2) with independently measured wire parameters, using either the measured zero-field critical temperature, T_{C0} , or equivalently, the spectroscopically measured zero-field superconducting gap, Δ_0 (Fig. S1 in the Supplemental Material [28]), which was consistent with the BCS relation $\Delta_0 = 1.76k_B T_{C0}$ [6]. Figure 2 demonstrates the remarkably good agreement found between experiment and theory. The observed increase of T_C with decreasing t_S is consistent with enhanced energy gaps for thin Al films [33].

Similar to the effects of flux-induced circumferential supercurrent, a dc current, I_S , applied along the wire can also drive the shell normal. The field-dependent critical current $I_C(\alpha)$ can be related to the corresponding critical temperature, $T_C(\alpha)$,

$$I_C(\alpha) = I_{C0} \left(\frac{T_C(\alpha)}{T_{C0}}\right)^{3/2}, \quad (3)$$

where I_{C0} is the zero-field critical current [34].

Base-temperature I_S - B_{\parallel} phase diagrams for wires A and B are shown in Fig. 3. The data are taken sweeping from negative to positive bias, so show retrapping currents for $I_S < 0$ and switching current for $I_S > 0$, both of which are proportional to the critical current, I_C [6]. Similar to the transition temperature, I_C was observed to be Φ_0 periodic in flux for both wires as expected from Eq. (3). For wire A, a

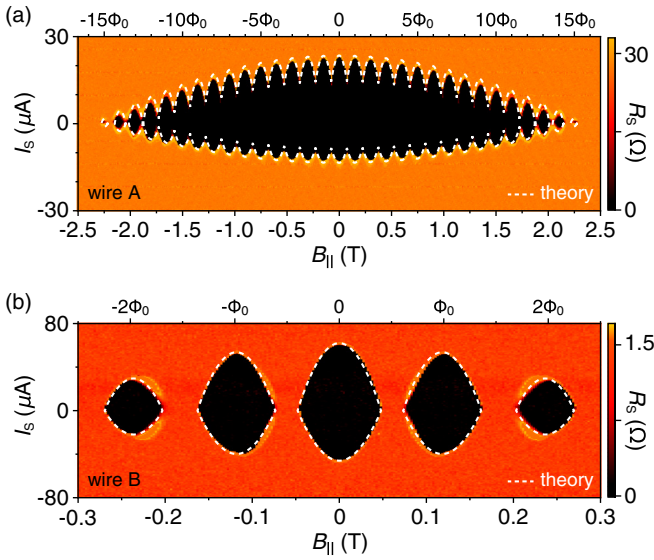


FIG. 3. (a) Shell resistance, R_S , measured for wire A with shell thickness $t_S = 7$ nm as a function of axial magnetic field, B_{\parallel} , and current bias, I_S . Both switching and retrapping currents are periodically modulated by B_{\parallel} up to $B_{\parallel,C} = 2.3$ T, whereafter the supercurrent is suppressed. The dashed theory curve is Eq. (3) evaluated with α_{\parallel} from Eq. (2) and the corresponding fit parameters measured for wire A. (b) Same as (a), but measured for wire B with shell thickness around $t_S = 25$ nm.

bigger range of B_{\parallel} [Fig. 3(a)] shows that the thin shell remains nondestructive up to ~ 2 T, corresponding to $\sim 13\Phi_0$, then enters the destructive regime twice around $14\Phi_0$ and finally turns fully normal around $B_{\parallel,C} = 2.3$ T.

Figure 3 shows theoretical curves based on Eqs. (1)–(3) superimposed on experimental data for both wire types. The zero-field switching and retrapping currents were taken as input parameters, with other parameters measured independently. Again, excellent agreement between experiment and theory for both thin (wire A) and thick (wire B) shells was found.

We next consider the effects of an applied *transverse* magnetic field, B_{\perp} , which can be used to control a crossover between conventional and destructive Little-Parks regimes. We investigate the combined effects of B_{\parallel} and B_{\perp} in wire C, with $d_C = 240$ nm and $t_S = 40$ nm. The larger diameter reduces the field value $B_{\parallel} = \Phi_0/A_F$ and the thicker shell ensures a long ξ_S , such that initially the wire is nearly destructive. The transition of the wire C from being nondestructive at $B_{\perp} = 0$ to destructive at $B_{\perp} = 13$ mT is depicted by I_S - B_{\parallel} phase diagrams in Figs. 4(a)–4(c).

Theoretically, the effect of B_{\perp} on the superconducting transition can be accounted for by introducing an additional pair-breaking term [3],

$$\alpha_{\perp} = \frac{4\xi_S^2 T_{C0}}{A_F} \frac{\Phi_{\perp}^2}{\Phi_0^2}, \quad (4)$$

where $\Phi_{\perp} = B_{\perp}A_F$. Figure 4 shows the theoretical transitions based on Eqs. (1)–(4) using $\alpha = \alpha_{\parallel} + \alpha_{\perp}$ [35] superimposed on experimental data.

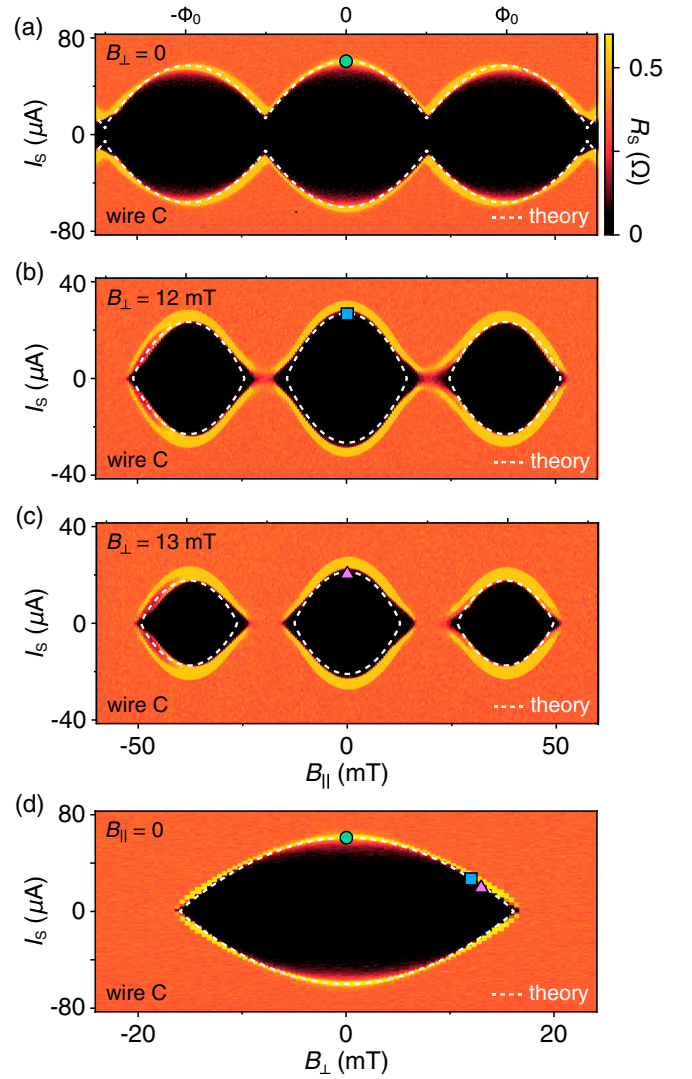


FIG. 4. (a) Base-temperature shell resistance, R_S , measured for wire C as a function of current bias, I_S , and parallel magnetic field, B_{\parallel} , at zero perpendicular magnetic field, $B_{\perp} = 0$. Approximately equal switching and retrapping currents, which are proportional to the critical current, indicate nearly dissipationless supercurrent injection. The wire is nondestructive throughout the whole measured B_{\parallel} range. (b) Same as (a), but at $B_{\perp} = 12$ mT. Around half-flux quantum and zero-current bias, an anomalous phase develops with a finite, but smaller than normal-state resistance. (c) Same as (a), but measured at $B_{\perp} = 13$ mT. Around the half-flux quantum R_S remains at normal-state value even at $I_S = 0$. The theory curves in (a)–(c) are Eq. (3) evaluated with $\alpha = \alpha_{\parallel} + \alpha_{\perp}$. (d) Critical current evolution as a function of B_{\perp} measured at $B_{\parallel} = 0$. The theory curve in (d) is Eq. (3) computed with α_{\perp} .

Near the conventional-destructive crossover [Fig. 4(b)], a resistive state with R_S smaller than R_N was observed around $\pm\Phi_0/2$ and $I_S = 0$. Figure 5 examines this resistive state close to the crossover, around $B_{\perp} \sim 12$ mT, along with superimposed theory curves based on Eqs. (1)–(4). Note that unlike the situation far from the crossover [Fig. 5(a)], where theory and experiment agree well, in the vicinity of the crossover [Figs. 5(b) and 5(c)] mean-field theory predicted T_C deviates from the temperatures where the shell displays R_N .

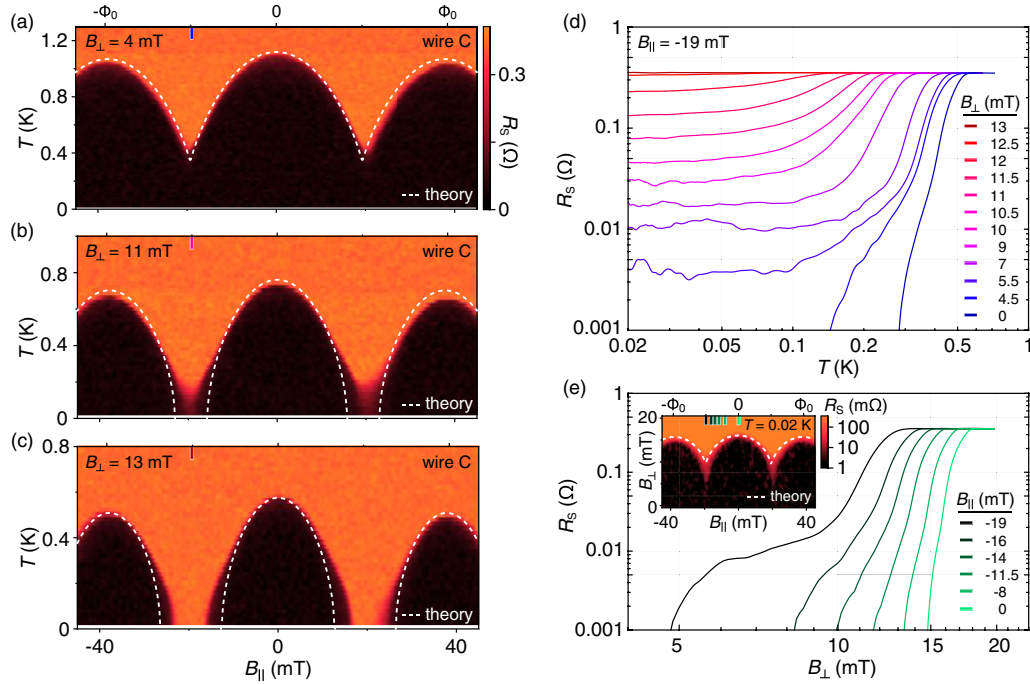


FIG. 5. (a) Differential shell resistance, R_S , measured for wire C at $B_{\perp} = 4$ mT as a function of temperature, T , and parallel magnetic field, B_{\parallel} . For small B_{\perp} the sample displays a nondestructive TB_{\parallel} phase diagram. (b) Same as (a), but measured at $B_{\perp} = 11$ mT. Around $\pm\Phi_0/2$ an anomalous-resistance phase develops at low T . (c) Same as (a), but measured at $B_{\perp} = 13$ mT. The shell resistance increases to the normal-state value as the applied flux passes $\pm\Phi_0/2$, even at the base temperature. Note that R_S is finite for all temperatures above the mean-field theory predicted T_C . The theory curves in (a)–(c) are Eq. (1) numerically solved for $T_C(\alpha_{\parallel} + \alpha_{\perp})$. (d) Half-flux quantum R_S as a function of T measured at different B_{\perp} values. Close to $B_{\perp} = 0$, as the temperature is lowered, the sample displays a conventional normal-superconducting phase transition. Around $B_{\perp} = 5$ mT the shell resistance at low T saturates to a finite, B_{\perp} -dependent value. Above $B_{\perp} = 13$ mT the shell resistance does not decrease below the normal-state resistance. (e) Base-temperature R_S as a function of B_{\perp} measured at different B_{\parallel} or Φ values. The resistance increases with B_{\perp} in a steplike manner with the step feature mostly pronounced at around $-\Phi_0/2$ of the applied flux. Inset: R_S as a function of B_{\perp} and B_{\parallel} . The theory curve was computed using Eq. (1), where a critical B_{\perp} was found for each B_{\parallel} , above which T_C vanishes.

Temperature dependence of R_S around $-\Phi_0/2$ for several values B_{\perp} near the conventional-destructive crossover are shown in Fig. 5(d). Throughout this regime, R_S was found to saturate to a temperature-independent value, which can be tuned over two orders of magnitude with small changes in B_{\perp} . In contrast, a R_S - T trace taken close to the second destructive regime, not near a crossover ($B_{\perp} = 12$ mT and $B_{\parallel} = 52$ mT) remains temperature dependent down to the base temperature (Fig. S2 in the Supplemental Material [28]). Qualitatively similar anomalous R_S saturation was also observed for different B_{\parallel} values at a fixed B_{\perp} (see Fig. S3 in the Supplemental Material [28]). At base temperature the evolution of R_S as a function of B_{\perp} shows a steplike increase that is mostly pronounced around $\pm\Phi_0/2$ [see Fig. 5(e)].

A possible explanation for the saturation of R_S in terms of disorder-induced variations of Δ , separating the shell into normal and superconducting segments [23], was tested by examining saturation effects in three segments of the same wire (Fig. S4 in the Supplemental Material [28]). It was found that all segments behaved the same, arguing against long-range variation in Δ on the scale of the separation of contacts. We also note that the anomalous resistance develops predominantly above the theoretical T_C , where the sample is expected to be in the normal state (Fig. S5 in the Supplemental Material [28]).

The steplike increase of R_S with B_{\perp} shown in Fig. 5(e) is reminiscent of phase slips, similar to the ones reported in Refs. [10,35], except here they are activated by perpendicular field rather than temperature. This suggests a picture in which anomalous saturating resistance results from quantum fluctuations not captured by mean-field theory. In general, the probability of a transverse phase slip across a weak link is proportional to $\exp(-R_Q/R_N)$, with the resistance quantum R_Q , and therefore is exponentially small for wire C [36]. However, near one-half-flux quantum, states with consecutive phase windings around the shell are degenerate, allowing quantum fluctuations to play a role. We note that both deep in the nondestructive regime [Fig. 2(a)] and deep in the destructive regime [Fig. 2(b)], no anomalous phase is observed.

Previous theoretical work [16,23] argued that the ratio of $d_{FTS}/2$ to λ^2 controls the order of the superconductor-metal transition. The present experiments span the range, with wires A and B having $d_{FTS}/2 < \lambda^2$, whereas wire C has $d_{FTS}/2 \gtrsim \lambda^2$. We have not observed systematic qualitative difference across this ratio. A detailed investigation of the order of the transition, and its affect on the anomalous metallic phase, would make an interesting future study.

In summary, we have investigated destructive and non-destructive Little-Parks effect in InAs nanowires fully

covered with epitaxial Al. Excellent agreement with Ginzburg-Landau mean-field theory was obtained across multiple reentrant quantum phase transitions using independently measured device and material parameters. Millitesla-scale perpendicular magnetic field was used to tune the crossover between destructive and nondestructive regimes, yielding an anomalous metallic phase around one-half-flux quantum with a temperature-independent resistance ranging over two orders of magnitude controlled by small changes in perpendicular field. This field-controllable anomalous phase is not explained

by existing theory, but presumably involves quantum fluctuations between winding numbers of superconducting phase around the cylindrical superconducting shell.

We thank Mingtang Deng, Claus Sørensen, and Shiv Upadhyay for materials and experimental contributions, and Mikhail Feigelman, Karsten Flensberg, Steve Kivelson, Yuval Oreg, Gil Refael, and Boris Spivak for valuable discussions. Research was supported by Microsoft, the Danish National Research Foundation, and the European Commission.

-
- [1] S. L. Sondhi, S. M. Girvin, J. P. Carini, and D. Shahar, *Rev. Mod. Phys.* **69**, 315 (1997).
- [2] T. Vojta, *Ann. Phys. (NY)* **9**, 403 (2000).
- [3] N. Shah and A. Lopatin, *Phys. Rev. B* **76**, 094511 (2007).
- [4] Q. Si and F. Steglich, *Science* **329**, 1161 (2010).
- [5] M. R. Norman, *Science* **332**, 196 (2011).
- [6] M. Tinkham, *Introduction to Superconductivity*, 2nd ed. (McGraw-Hill, New York, 1996).
- [7] A. Del Maestro, B. Rosenow, and S. Sachdev, *Ann. Phys. (NY)* **324**, 523 (2009).
- [8] A. M. Goldman, *Int. J. Mod. Phys. B* **24**, 4081 (2010).
- [9] A. Kapitulnik, S. A. Kivelson, and B. Spivak, *Rev. Mod. Phys.* **91**, 011002 (2019).
- [10] A. Bezryadin, C. N. Lau, and M. Tinkham, *Nature (London)* **404**, 971 (2000).
- [11] A. D. Zaikin, D. S. Golubev, A. van Otterlo, and G. T. Zimányi, *Phys. Rev. Lett.* **78**, 1552 (1997).
- [12] O. V. Astafiev, L. B. Ioffe, S. Kafanov, Yu. A. Pashkin, K. Yu. Arutyunov, D. Shahar, O. Cohen, and J. S. Tsai, *Nature (London)* **484**, 355 (2012).
- [13] J. E. Mooij and C. J. P. M. Harmans, *New J. Phys.* **7**, 219 (2005).
- [14] B. S. Deaver, Jr. and W. M. Fairbanks, *Phys. Rev. Lett.* **7**, 43 (1961).
- [15] H. Doll and M. Näbauer, *Phys. Rev. Lett.* **7**, 51 (1961).
- [16] D. H. Douglass, Jr., *Phys. Rev.* **132**, 513 (1963).
- [17] W. A. Little and R. D. Parks, *Phys. Rev. Lett.* **9**, 9 (1962).
- [18] P.-G. de Gennes, *C. R. Acad. Sci. Paris* **292**, 279 (1981).
- [19] R. M. Arutyunyan and G. F. Zharkov, *Zh. Eksp. Teor. Fiz.* **79**, 245 (1980) [*Sov. Phys. JETP* **52**, 124 (1980)].
- [20] G. Schwiete and Y. Oreg, *Phys. Rev. Lett.* **103**, 037001 (2009).
- [21] Y. Liu, Yu. Zadorozhny, M. M. Rosario, B. Y. Rock, P. T. Carrigan, and H. Wang, *Science* **294**, 2332 (2001).
- [22] I. Sternfeld, E. Levy, M. Eshkol, A. Tsukernik, M. Karpovski, H. Shtrikman, A. Kretinin, and A. Palevski, *Phys. Rev. Lett.* **107**, 037001 (2011).
- [23] V. H. Dao and L. F. Chibotaru, *Phys. Rev. B* **79**, 134524 (2009).
- [24] O. Vafeek, M. R. Beasley, and S. A. Kivelson, *arXiv:cond-mat/0505688*.
- [25] A. V. Lopatin, N. Shah, and V. M. Vinokur, *Phys. Rev. Lett.* **94**, 037003 (2005).
- [26] P. Krogstrup, N. L. B. Ziino, W. Chang, S. M. Albrecht, M. H. Madsen, E. Johnson, J. Nygård, C. M. Marcus, and T. S. Jespersen, *Nat. Mater.* **14**, 400 (2015).
- [27] S. Vaitiekėnas, M.-T. Deng, P. Krogstrup, and C. M. Marcus, *arXiv:1809.05513*.
- [28] See Supplemental Material at <http://link.aps.org/supplemental/10.1103/PhysRevB.101.060507> for more detailed device description and additional measurements, see also Ref. [29].
- [29] C. Kittel, *Introduction to Solid State Physics*, 8th ed. (Wiley, New York, 2005).
- [30] A. E. G. Mikkelsen, P. Kotetes, P. Krogstrup, and K. Flensberg, *Phys. Rev. X* **8**, 031040 (2018).
- [31] A. E. Antipov, A. Bargerbos, G. W. Winkler, B. Bauer, E. Rossi, and R. M. Lutchyn, *Phys. Rev. X* **8**, 031041 (2018).
- [32] A. A. Abrikosov and L. P. Gor'kov, *Zhur. Eksptl'. i Teoret. Fiz.* **39**, 1781 (1960) [*Sov. Phys. JETP* **12**, 1243 (1961)].
- [33] N. A. Court, A. J. Ferguson, and R. G. Clark, *Supercond. Sci. Technol.* **21**, 015013 (2008).
- [34] J. Bardeen, *Rev. Mod. Phys.* **34**, 667 (1962).
- [35] A. Rogachev, A. T. Bollinger, and A. Bezryadin, *Phys. Rev. Lett.* **94**, 017004 (2005).
- [36] M. Vanević and Y. V. Nazarov, *Phys. Rev. Lett.* **108**, 187002 (2012).